Journal of ELECTRONIC MATERIALS, Vol. 48, No. 4, 2019
https://doi.org/10.1007/s11664-019-06963-8

Temperature-Dependent Electrical Characteristics and Extraction of Richardson Constant from Graphitic-C/*n*-Type 6H-SiC Schottky Diodes

HUNG PHAM ,[1,2] HIEP N. TRAN,[1] ANTHONY S. HOLLAND,[1] and JIM G. PARTRIDGE[3,4]

1.—School of Engineering, RMIT University, GPO Box 2476V, Melbourne, VIC 3001, Australia. 2.—School of Science and Technology, RMIT University, Ho Chi Minh City, Vietnam. 3.—School of Science, RMIT University, GPO Box 2476V, Melbourne, VIC 3001, Australia. 4.—e-mail: jim.partridge@rmit.edu.au

Energetically deposited graphitic carbon (C) is known to form high-endurance rectifying contacts to a variety of semiconductors. Graphitic contacts to *n*-type 6H-SiC have demonstrated current rectification ratios (at ± 1.5 V) up to 1:10^6. In this article, the current voltage temperature (*I*–*V*–*T*) characteristics of these devices are examined to reveal more detail on the junction/barrier properties that are critical to performance. Analysis of the *I*–*V*–*T* characteristics and disparity between barrier heights extracted from the *I*–*V*–*T* data and *C*–*V* data show inhomogeneity in the contacts and this has been quantified. Accounting for the inhomogeneity, the homogeneous Richardson constant of the *n*-type 6H-SiC can be extracted from the *I*–*V*–*T* data, and this value agrees with the reported theoretical value.

Key words: Graphenic carbon, graphitic carbon, electronic materials, Schottky contacts

INTRODUCTION

Silicon carbide is a wide band gap semiconductor that exhibits low dielectric constant, high thermal conductivity, high breakdown electric field and high saturation velocity.[1] It is extensively employed in high-power electronics.[2,3] Of the three main polytypes (4H-SiC, 6H-SiC and 3C-SiC[3]), 6H-SiC is the most widely used, with established and emerging applications in optoelectronics, high-power/high-temperature electronics and non-volatile memory.[4] In all devices based on 6H-SiC, electrical contacts are crucial, and improved methods for fabricating these contacts are under continual development.[5,6] Rectifying contacts, necessary in many power devices, often endure high current densities and operational temperatures. These conditions are sometimes sufficient to cause significant deterioration in performance.[7] Carbon-based contacts exhibit excellent electrical properties and superior stability when compared with conventional metal/alloy alternatives.[7] In addition, the electrical characteristics of carbon can be tuned by manipulating microstructure, dopant levels and/or by using nano-dimensional forms such as graphene.[8–11] High-performance rectifying carbon contacts to 6H-SiC have been formed using bulk graphite,[12] colloidal graphite,[13] graphenic material[8,14] and graphitic thin films deposited from energetic plasmas.[6,15] The latter approach is compatible with optical lithography, enabling accurate placement and dimensioning of contacts on the 6H-SiC substrate.

In this work, temperature-dependent current–voltage (*I*–*V*–*T*) and capacitance–voltage (*C*–*V*) characteristics have been collected from energetically deposited, lithographically defined C/6H-SiC contacts,[6] while the barrier height, ideality factor and Richardson constant have been extracted from the measurement data. In addition, we use an

(Received October 1, 2018; accepted January 12, 2019; published online January 23, 2019)

approach similar to that adopted by Sarpatwari et al.[16] to investigate the effects of lateral inhomogeneity on these parameters and to arrive at modified values based on laterally homogeneous C/6H-SiC devices.

EXPERIMENTAL

Prior to deposition, an n-type 6H-SiC wafer (with a room-temperature n-type carrier concentration of 2×10^{17} cm^{-3} and electron mobility of 76 cm^2/Vs) was diced into 10×10 mm^2 substrates. These substrates were cleaned with acetone and isopropanol before a 1-μm-thickness layer of AZ1512 photoresist was applied. No native oxide etch was performed. The contact patterns (arrays of 200-μm-diameter apertures) were exposed using a Karl Suss MJB-3 mask aligner before being developed. The substrates were then mounted on a heater/holder a 200°C in a filtered cathodic vacuum arc (FCVA; Nanofilm) system that was pumped to a base pressure lower than 7×10^{-7} kPa. A 60-A arc current was established to ablate a 68-mm-diameter 99.99% purity carbon cathode. The energy of the depositing flux was controlled with a DC voltage, set to 1.0 kV. The majority of the C ions generated by the FCVA system are known to be singly charged[6] and the maximum kinetic energy of the depositing singly charged ions was therefore 1.0 keV. This incident energy promoted the formation of sp^2 bonds and extended oriented graphitic planes within the film/contacts.[6,17,18] Deposition rates were 10 nm/min and the C film thickness was 40–50 nm. Finally, to assist with optical contrast for probing, a Pt layer (thickness 20 nm) was deposited on top of the C layer. The schematic inset in Fig. 1 illustrates the device structure.

Current voltage (I–V) characterization was performed using a probe-station and a Keysight B2902A power source connected to a computer.

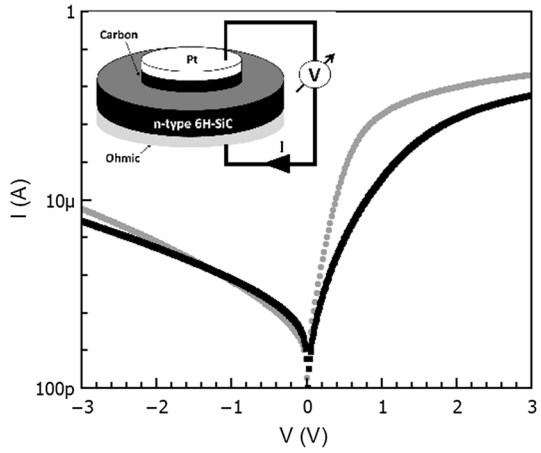

Fig. 1. I–V characteristics of energetically deposited C/6H-SiC diodes with direct bias (gray) and remote bias (black) applied during deposition, and (inset) schematic of the device measurement circuit.

The operating temperature was varied from 98 to 498 K using a Linkam PE95 temperature controller and liquid nitrogen-cooled test chamber equipped with miniature electrical probe arms. The room-temperature capacitance–voltage measurements were conducted at a frequency of 1.00 MHz using a Boonton 7200 capacitance meter.

RESULTS AND DISCUSSION

Figure 1 shows the measurement circuit (inset) and the I–V characteristics measured at room temperature from two C/6H-SiC devices, both 200 μm in diameter. These devices differ in how the substrate bias was applied during C deposition. The data shown in gray originates from a device deposited with the 1.0-kV bias applied directly to the substrate holder. The black curve originates from a device deposited with the 1.0-kV bias applied remotely to a conducting carbon-coated mesh in front of the substrate (with the substrate at floating potential).[19] The latter produces a broader distribution of ion energies, with more ions arriving at the substrate with lower energy. This lower average energy has resulted in a rectifying device but not a Schottky barrier device, since the I–V characteristic is non-linear at low forward bias in the semi-logarithmic I–V plot. Alternative fitting (not shown) indicates that a field-independent barrier exists in this device which then consequently resembles a metal–insulator–semiconductor diode. In this structure, it is likely that the insulator is an interfacial oxygen-rich layer, since the native oxide on the 6H-SiC was not removed prior to C deposition.

The device formed with direct bias exhibits linearity at low forward bias and its characteristics can be fitted well assuming thermionic emission (TE) over a Schottky barrier.[20] From both device characteristics, we can extract various room-temperature device parameters. Firstly, the rectification ratios at $\pm$ 1.5 V are, respectively, 2 k and 10 k for the remote and direct DC biased devices, while their series resistances are 170 Ω and 80 Ω. The ideality factor of the direct bias deposited device is 1.8, significantly closer to unity than the ideality factor of the device deposited with remote bias (3.1). This is consistent with the differing dominant transport mechanisms in the two devices. Ideality factors between 1 and 2 are generally taken as indicative of TE over a Schottky barrier.[20] The differences in the device parameters show that the energy of deposition plays a significant role in the device characteristics. Transmission electron microscopy has been used to show that energetic C fluxes can remove native oxide layers from device interfaces as deposition takes place,[17,18] and we attribute the Schottky behavior of the direct biased device to this effect. Finally, the apparent (room-temperature) barrier heights are 0.67 and 0.71 eV with the higher value belonging to the device deposited with direct bias.

Following the room-temperature measurements, *I–V–T* characterization was performed on the (direct biased) C/6H-SiC Schottky barrier device to further investigate its electrical properties. The 0–0.5 V forward bias portions of the temperature dependent *I–V* characteristics from this device (measured from 98 K to 498 K) are shown in Fig. 2a. All characteristics are shown with linear fits, corresponding to TE over a Schottky barrier.

Assuming TE, the forward current–voltage (*I–V*) characteristics of the rectifying C/6H-SiC diode are expressed by:

$$I = I_s \exp\left[\left(\frac{q(V - IR_s)}{nkT}\right) - 1\right] \quad (1)$$

where I is the current, T the temperature, q the electron charge, k the Boltzmann constant, n the ideality factor, V the applied voltage, R_s the series resistance, and I_s the saturation current, given by:

$$I_s = AA^*T^2 \exp\left(-\frac{q\Phi_B}{kT}\right) \quad (2)$$

where A is the contact area, A^* the Richardson constant with theoretical value of 194 A cm^{-2} K^{-2},[21] and Φ_B the barrier height.

The temperature-dependent differential device resistance (R_{diff}=dV/dI) is shown in Fig. 2b. The series resistance of the device, R_s, is determined from each curve at saturation and ranges from 48 Ω at 498 K to 1.18 kΩ at 98 K. The dominant contribution to this series resistance is from the bulk 6H-SiC substrate and (as shown in the Fig. 2 inset) is proportional to $-E_A/kT$ where E_A is the energy difference between the active donor level and conduction band of the *n*-type 6H-SiC.[22] Here, E_A is equal to 0.032 ± 0.002 eV.

Next, we re-evaluated the rectification ratio, barrier height and ideality factors based on the *I–V–T* characteristics (see Fig. 3). The temperature-dependent *I–V* characteristics and rectification ratio are shown in Fig. 3a and b, respectively. The reverse device current (number of charge carriers overcoming the barrier) increases appreciably as the temperature is increased.[8] The rectification ratio, calculated from fixed bias voltage of ± 1.5 V, is therefore maximum (~ 10^6) at the minimum temperature (98 K), while at room temperature, it exceeds 10^4. This reduction of rectification ratio is at least in part due to narrowing of the depletion region in the 6H-SiC as the carrier concentration in the 6H-SiC increases with increased temperature. Since the depletion width in a Schottky diode is inversely proportional to the square root of the carrier concentration in the semiconductor,[20] increasing the temperature leads to increased carrier concentration and a reduction in the depletion layer width. In reverse bias, a narrower depletion region enables a substantially increased reverse tunnelling current. This reduces the calculated rectification ratio since the forward current is dominated by thermionic emission and hence increases less significantly with increased tunnelling. This is most clearly seen in the combined forward and reverse bias *I–V–T* plot shown in Fig. 3a.

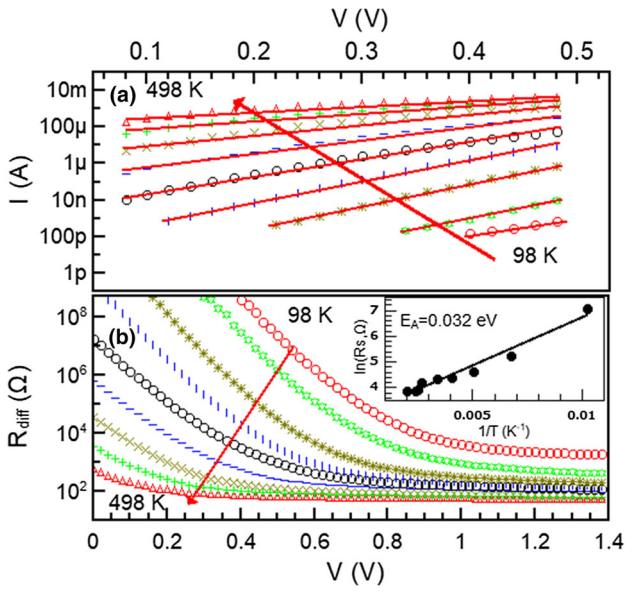

Fig. 2. (a) Forward bias portions of the *I–V–T* characteristics of the C/6H-SiC Schottky diode with linear fits showing transport by TE, and (b) temperature-dependent differential device resistance versus voltage characteristics. The energy difference between the donor level and conduction band in the *n*-type 6H-SiC substrate is determined from the inset Arrhenius plot.

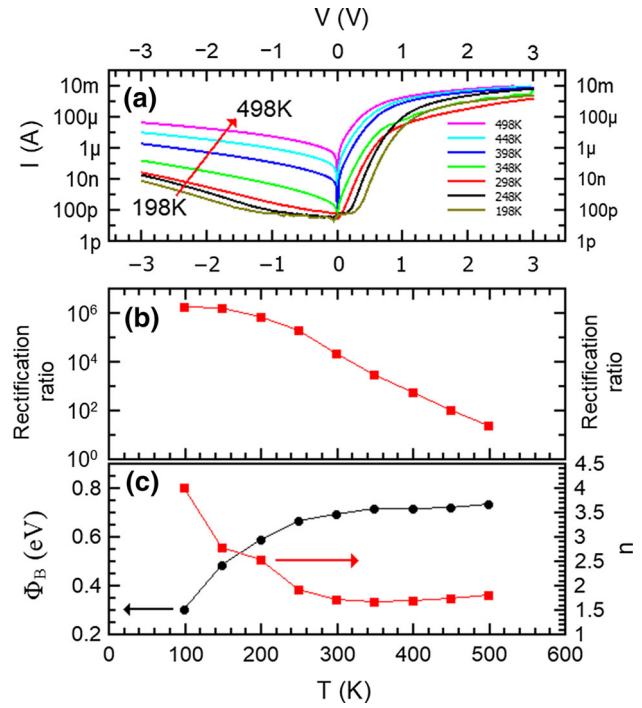

Fig. 3. Temperature-dependent (a) *I–V* characteristics, (b) rectification ratios, and (c) ideality factors/apparent barrier heights of a C/6H-SiC diode.

Referring to Eq. 1, the barrier height and ideality factor at each temperature are determined from:

$$\phi_B = \frac{kT}{q}\ln\left(\frac{AA^*T^2}{I_s}\right) \quad (3)$$

and

$$n = \frac{q}{kT}\frac{dV}{d(\ln I)} \quad (4)$$

as shown in Fig. 3c.

Figure 3c shows that the barrier appears to increase with elevated temperature. This is again indicative of barrier inhomogeneity.[23,24] If the contact exhibits location-dependent interface properties, then it can be viewed as an array of patches with differing barrier heights.[25] At lower temperatures, a larger fraction of the total device current will come from carriers crossing patches with lower barrier heights, and therefore the apparent barrier height will decrease (as shown in Fig. 3c). The ideality factor increases as the temperature decreases, since a greater proportion of the (smaller) device current results from carriers transported by mechanisms other than TE.

Capacitance–voltage (C–V) characterization was performed to further investigate the properties of the interface/barrier in the C/6H-SiC devices. The 'true' capacitance (C) is evaluated using the formula[26,27]:

$$C = \left[\frac{C_m^{-2} - 2R_s^2\omega^2 - \sqrt{\left(C_m^{-2} - 2R_s^2\omega^2\right)^2 - 42R_s^4\omega^4}}{2R_s^4\omega^4}\right]^{1/2} \quad (5)$$

where C_m is measured capacitance, R_s the device series resistance, and ω the angular frequency.

The room temperature $1/C^2$ versus V relationship (not shown) was linear over the reverse bias measurement range, but the barrier height obtained from these measurements significantly exceeded that calculated from the room-temperature I–V measurements (1.46 eV versus 0.7 eV). According to Tung's model,[25] this can be explained by the presence of barrier inhomogeneity, since, during the I–V measurements, current transport occurs mainly over the low Schottky barrier height 'patches' within the larger device area.[25,28] Thus, the discrepancy in barrier heights determined from the I–V and C–V measurements is consistent with the presence of lateral inhomogeneity and provides further justification for investigation of this effect. Figure 4a shows the reverse bias I–V–T characteristic of C/6H-SiC diodes at $3\text{ V} > |V| > 0.6\text{ V}$. When Schottky emission is the dominant transport mechanism, the current is described by[29]:

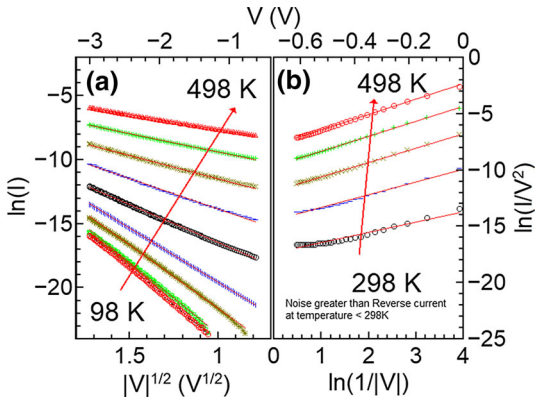

Fig. 4. The temperature-dependent current voltage characteristics of C/6H-SiC diodes with reverse bias voltages of (a) $3\text{ V} > |V| > 0.6\text{ V}$ and (b) $0.6\text{ V} > |V| > 0\text{ V}$. The linearities in (a) and (b) are consistent with transport dominated by Schottky emission and direct tunnelling, respectively.

$$I \propto T^2 \exp\left(\frac{q}{2kT}\sqrt{\frac{qV}{\pi\epsilon\epsilon_o d}}\right) \quad (6)$$

where ϵ is the relative permittivity, ϵ_o is the permittivity of free space and ϵ_o is the thickness of the potential barrier.

The Schottky emission plot shown in Fig. 4a exhibits linearity throughout the reverse voltage region and across all measurement temperatures. Current over the lowered barrier is therefore dominant. Similar characteristics in the reverse bias region have been reported in Ti/Ni/SiC,[30] CdS,[31] Au/GaAs,[32] Au/PMI/n-Si and Al/ZnO/Au Schottky diodes.[33–35] As shown in Fig. 4b, the dominant transport mechanism in the region $|V| < 0.6\text{ V}$ is described by the direct tunnelling equation[36]:

$$\ln\left(\frac{I}{V^2}\right) \propto \ln\left(\frac{1}{V}\right) - \frac{2d\sqrt{2m_e\phi_B}}{\hbar} \quad (7)$$

where m_e is electron effective mass and $\hbar$ is Planck's constant divided by 2π.

In junctions with significant inhomogeneity, regions ('patches') within the total junction area may exhibit barriers thin enough to enable such a tunnelling current.[37]

With confirmed barrier inhomogeneity, we follow the approach reported by Sarpatwari et al.[16] to extract the effective values of Richardson constant A^*_{eff} and barrier height Φ_{Beff}, using the following relationship:

$$\ln\left(\frac{I_s}{AT^2}\right) = -\frac{q\Phi_{Beff}}{kT} + \ln\left(A^*_{eff}\right) \quad (8)$$

which includes saturation currents (I_s) extracted from device I–V measurements and the device area (A). A plot of this relationship (Fig. 5a) provides values for A^*_{eff} of 0.45 A cm^{-2} K^{-2} and Φ_{Beff} of 0.52 eV. The A^*_{eff} value is significantly less than the reported A^* value for 6H-SiC of 194 A cm^{-2} K^{-2},[21]

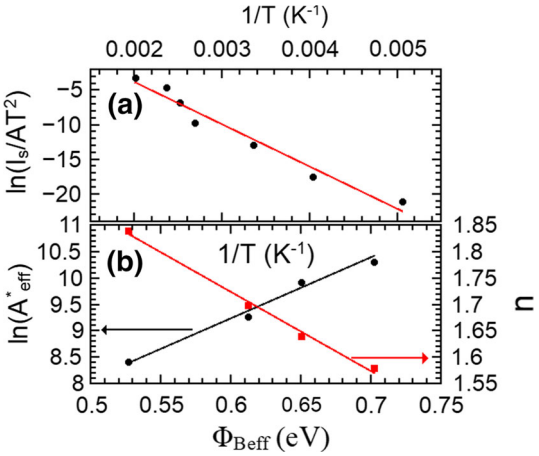

Fig. 5. (a) Richardson plot constructed from the *I–V–T* data of the C/6H-SiC Schottky diode, and (b) linear correlation between $\ln(A^*_{\text{eff}})$ and Φ_{Beff} obtained from several devices and the Φ_{Beff} versus n relationship used to determine the barrier height characteristic of a laterally homogeneous energetically deposited C/6H-SiC Schottky diode.

while Φ_{Beff} is also significantly lower than the barrier height calculated from our *I–V–T* data. Similar disparity has been reported in numerous Schottky diodes based on a variety of materials[38,39] and once again lateral inhomogeneity of the junction is a known cause. It is reasonable to assume that this is the case when the device ideality factor (n) exceeds 1.3.[16,37] The relationship between A^*_{eff} and Φ_{Beff} is described by[16]:

$$\ln\left(A^*_{\text{eff}}\right) = \ln\left(A^*_o\right) + \left(\beta - \frac{1}{\beta\beta_1^2\sigma^2}\right)\left(\Phi_{\text{Beff}} - \Phi_{\text{Bo}}\right) \quad (9)$$

where A^*_o and Φ_{Bo} are the homogeneous Richardson constant and barrier height, respectively, β equals q/kT, β_1 equals $(V_{\text{bb}}/\eta)^{1/3}$ with the V_{bb} term being the band bending at the measurement bias and $\eta = \epsilon_s/qN_D$ the doping density-dependent parameter.[25] Parameter η determines the overall patch strength and at higher doping levels (low η), conduction through the low barrier regions is enhanced. From Eq. 7, we construct the plot in Fig. 5b which exhibits a linear relationship between $\ln(A^*_{\text{eff}})$ and Φ_{Beff}. As the barrier height becomes more homogeneous, A^*_{eff} and Φ_{Beff} move closer to A^*_o and Φ_{Bo}. To determine Φ_{Bo}, the Φ_{Beff} versus n plot is extrapolated to $n = 1.05$ (the lowest reported ideality factor for a Schottky contact to 6H-SiC[37,40,41]) to yield $\Phi_{\text{Bo}} = 1.05 \pm 0.015$ eV. This Φ_{Bo} is then used to extract a homogeneous Richardson constant A^*_o of 187 ± 42 A cm^{-2} K^{-2}. This range encompasses the theoretical value of 194 A cm^{-2} K^{-2}.

CONCLUSION

The temperature-dependent electrical properties of energetically deposited C/6H-SiC Schottky diodes have been studied. Lateral inhomogeneity of the junction/barrier manifests itself in the *I–V–T* characteristics and causes disparity between barrier heights determined from the *I–V* and *C–V* measurements. Using established methods, and from the relationships between barrier height and ideality factor and barrier height versus Richardson constant, the homogeneous barrier height and Richardson constant were calculated from the measurement data. The calculated Richardson constant (187 ± 42 A cm^{-2} K^{-2}) agreed with the theoretical value of 194 A cm^{-2} K^{-2} for n-type 6H-SiC. This work demonstrates the potential to form high-performance Schottky contacts to 6H-SiC using energetically deposited carbon, but shows that high lateral homogeneity across the junctions of these devices is vital in achieving higher rectification and ideality factors approaching unity.

REFERENCES

1. J. Biela, M. Schweizer, S. Waffler, B. Wrzecionko, and J.W. Kolar, *Mater. Sci. Forum* 645–648, 1101 (2010).
2. S. Dimitrijev, *Microelectron. Eng.* 83, 123 (2006).
3. M. Bhatnagar and B.J. Baliga, *IEEE Trans. Electron Devices* 40, 645 (1993).
4. J.W. Palmour, J.A. Edmond, H.S. Kong, and C.H. Carter, *Phys. B* 185, 461 (1993).
5. S. Hertel, D. Waldmann, J. Jobst, A. Albert, M. Albrecht, S. Reshanov, A. Schöner, M. Krieger, and H.B. Weber, *Nat. Commun.* 3, 957 (2012).
6. M. Kracica, E.L.H. Mayes, H.N. Tran, A.S. Holland, D.G. McCulloch, and J.G. Partridge, *Carbon* 102, 141 (2016).
7. M. Stelzer and F. Kreupl, in *2016 IEEE International Electron Devices Meeting (IEDM)* (2016), pp. 21.7.1–21.7.4.
8. A. Di Bartolomeo, *Phys. Rep.* 606, 1 (2016).
9. E.L.H. Mayes, D.G. McCulloch, and J.G. Partridge, *Appl. Phys. Lett.* 103, 182101 (2013).
10. W. Lu, W.C. Mitchel, C.A. Thornton, W.E. Collins, G.R. Landis, and S.R. Smith, *J. Electrochem. Soc.* 150, G177 (2003).
11. J. Crofton, P.G. McMullin, J.R. Williams, and M.J. Bozack, *J. Appl. Phys.* 77, 1317 (1995).
12. T. Seyller, K.V. Emtsev, F. Speck, K.Y. Gao, and L. Ley, *Appl. Phys. Lett.* 88, 242103 (2006).
13. S. Tongay, T. Schumann, and A.F. Hebard, *Appl. Phys. Lett.* 95, 222103 (2009).
14. S. Huebner, N. Miyakawa, S. Kapser, A. Pahlke, and F. Kreupl, *IEEE Trans. Nucl. Sci.* 62, 588 (2015).
15. J.C. Angus, P. Koidl, and S. Domitz, *Plasma Deposited Thin Films* (Boca Raton: CRC Press, 2018), pp. 89–127.
16. K. Sarpatwari, O.O. Awadelkarim, M.W. Allen, S.M. Durbin, and S.E. Mohney, *Appl. Phys. Lett.* 94, 242110 (2009).
17. D.W.M. Lau, D.G. McCulloch, M.B. Taylor, J.G. Partridge, D.R. McKenzie, N.A. Marks, E.H.T. Teo, and B.K. Tay, *Phys. Rev. Lett.* 100, 176101 (2008).
18. D.W.M. Lau, J.G. Partridge, M.B. Taylor, D.G. McCulloch, J. Wasyluk, T.S. Perova, and D.R. McKenzie, *J. Appl. Phys.* 105, 084302 (2009).
19. A. Moafi, D.W.M. Lau, A.Z. Sadek, J.G. Partridge, D.R. McKenzie, and D.G. McCulloch, *J. Appl. Phys.* 109, 073309 (2011).
20. S.M. Sze and K.K. Ng, *Physics of Semiconductor Devices*, 3rd ed. (Hoboken: Wiley, 2006).
21. T. Teraji, S. Hara, H. Okushi, and K. Kajimura, *Appl. Phys. Lett.* 71, 689 (1997).
22. W.P. Kang, J.L. Davidson, Y. Gurbuz, and D.V. Kerns, *J. Appl. Phys.* 78, 1101 (1995).
23. J.H. Werner and H.H. Güttler, *J. Appl. Phys.* 73, 1315 (1993).
24. J.P. Sullivan, R.T. Tung, M.R. Pinto, and W.R. Graham, *J. Appl. Phys.* 70, 7403 (1991).

25. R.T. Tung, *Phys. Rev. B* 45, 13509 (1992).
26. M.M. Solovan, N.M. Gavaleshko, V.V. Brus, A.I. Mostovyi, P.D. Maryanchuk, and E. Tresso, *Semicond. Sci. Technol.* 31, 105006 (2016).
27. M.N. Solovan, G.O. Andrushchak, A.I. Mostovyi, T.T. Kovaliuk, V.V. Brus, and P.D. Maryanchuk, *Semiconductors* 52, 236 (2018).
28. J.H. Werner and H.H. Güttler, *J. Appl. Phys.* 69, 1522 (1991).
29. H.-D. Lee, *IEEE Trans. Electron Devices* 47, 762 (2000).
30. K.P. Schoen, J.M. Woodall, J.A. Cooper, and M.R. Melloch, *IEEE Trans. Electron Devices* 45, 1595 (1998).
31. R. Zuleeg and R.S. Muller, *Solid State Electron.* 7, 575 (1964).
32. F.A. Padovani, *Solid State Electron.* 11, 193 (1968).
33. Ö.F. Yüksel, M. Kuş, N. Şimşir, H. Şafak, M. Şahin, and E. Yenel, *J. Appl. Phys.* 110, 024507 (2011).
34. K.H. Yoo, K.S. Kang, Y. Chen, K.J. Han, and J. Kim, *Appl. Phys. Lett.* 93, 192113 (2008).
35. K.J. Han, K.S. Kang, Y. Chen, K.H. Yoo, and K. Jaehwan, *J. Phys. D Appl. Phys.* 42, 125110 (2009).
36. J.M. Beebe, B. Kim, J.W. Gadzuk, C.D. Frisbie, and J.G. Kushmerick, *Phys. Rev. Lett.* 97, 026801 (2006).
37. L. Zheng, R.P. Joshi, and C. Fazi, *J. Appl. Phys.* 85, 3701 (1999).
38. F. Roccaforte, F.L. Via, V. Raineri, R. Pierobon, and E. Zanoni, *J. Appl. Phys.* 93, 9137 (2003).
39. A.F. Hamida, Z. Ouennoughi, A. Sellai, R. Weiss, and H. Ryssel, *Semicond. Sci. Technol.* 23, 045005 (2008).
40. M. Bhatnagar, B.J. Baliga, H.R. Kirk, and G.A. Rozgonyi, *IEEE Trans. Electron Devices* 43, 150 (1996).
41. C. Raynaud, K. Isoird, M. Lazar, C.M. Johnson, and N. Wright, *J. Appl. Phys.* 91, 9841 (2002).